Annals Geol. Surv. Egypt. XL (2024). pp. 120- 135
Manuscript ID: ASGE-2405-1012

Structural Mapping and Groundwater Geophysical Exploration of Al-Himma Village and Its Surrounding Area, North of Minya Governorate, Egypt

By
Mohamed Elsadek M. Sabra[1]* and Ahmed Abdel Aziz[2]
1. Egyptian Mineral Resources Authority, Po. Box 11517, Abbassiya, Cairo, Egypt
2. Geology Department, Faculty of Science, Kafr Elsheikh University, Egypt
muhamed.elsadek@yahoo.com

ABSTRACT

The city of Matay is located at the eastern bank of the Nile River, about 41 km to the north of Minya City. Matay is one of the villages of Minya Governorate. Digital elevation model (DEM) was used to identify the lineaments, which extend mainly in the NW-SE, N-S and NE-SW directions. The extracted lineaments from the geologic maps strike in the NW-SE and NE-SW directions, while those extracted from the magnetic maps strike in the N-S, E-W, NE-SW and NW-SE directions. Three vertical electrical sounding (VES) were acquired in the study area, and data from drilled well in the study area used to identify the occurrence of the groundwater. The drilled well confirmed the water depths obtained from vertical electrical soundings. The water level starts below 12.5 m at this drilled well. Subsurface lithology of the study area consists of four layers as follow; unconsolidated wadi sediments, clay stone layer, intercalation of sand and clay layer, and saturated limestone layer.
Key words: Digital Elevation Model, Lineaments, Vertical Electrical Sounding and Aquifer.

INTRODUCTION

The study area (Al-Himma Village) is located at the northern part of Minya Governorate and lies between longitudes 30° 10′ 00″ E and 30° 50′ 00″ E and latitudes 28° 10′ 00″ N and 28° 50′ 00″ N (Fig.1). This area has been intensively investigated by many workers (e.g. Abdelaal et al 2017; Gedamy et al 2019; Abouelmaged et al., 2020; Abdullah & Ahmed 2021; Moftah et al 2022; Darwish, 2023 and Asmoay et al., 2024). Structural lineaments have long been used in water resource investigations. The current study aims to delineate the surface and subsurface structural framework and to identify groundwater occurrence in the considered area.

The groundwater plays an important role for developments and encouragement of investments in areas far from surface running freshwater. Hence, it was necessary to conduct this research to explore chances of development of the study area.

GEOLOGIC SETTING

The different rock units in the study area (Fig. 2) comprise the following: A) Igneous rocks, which represented by basaltic dykes, sills and flows). B) Tertiary sedimentary rocks that include the following units; i) Minya Formation (lower Eocene); represented by limestone with A. frumentiformis in the upper part. Local patchreefs. Base grades into nummulitic lower Eocene to the south and east. ii) Mokattam Group (lower to middle Eocene); consists of Samalut and Wadi Rayan formations and represented by marine limestone. iii) Gabal Qatrani Formation (Oligocene); comprises a series of clastic rocks of siltstone and claystone. C) Quaternary deposits; which consist of gravel, sand dunes, and Nile deposits (Conoco, 1987). Several fault trends and fractures have been recorded (Fig. 3), which include the following trends; NW-SE and NE-SW that plays an important role in recharging the limestone aquifer of the middle Eocene (Shabana, 2010).

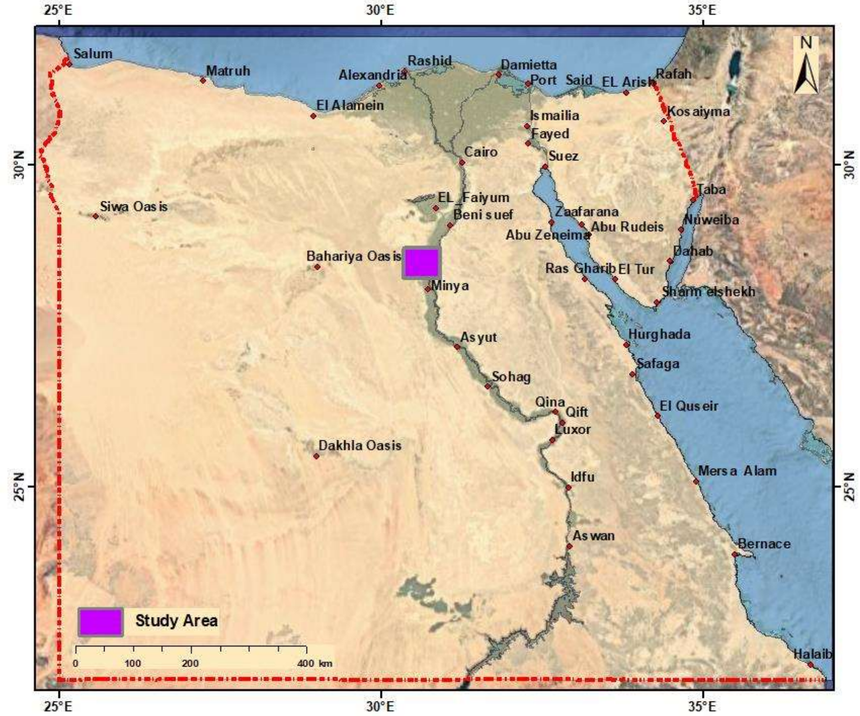

Figure 1: Location map of the study area.

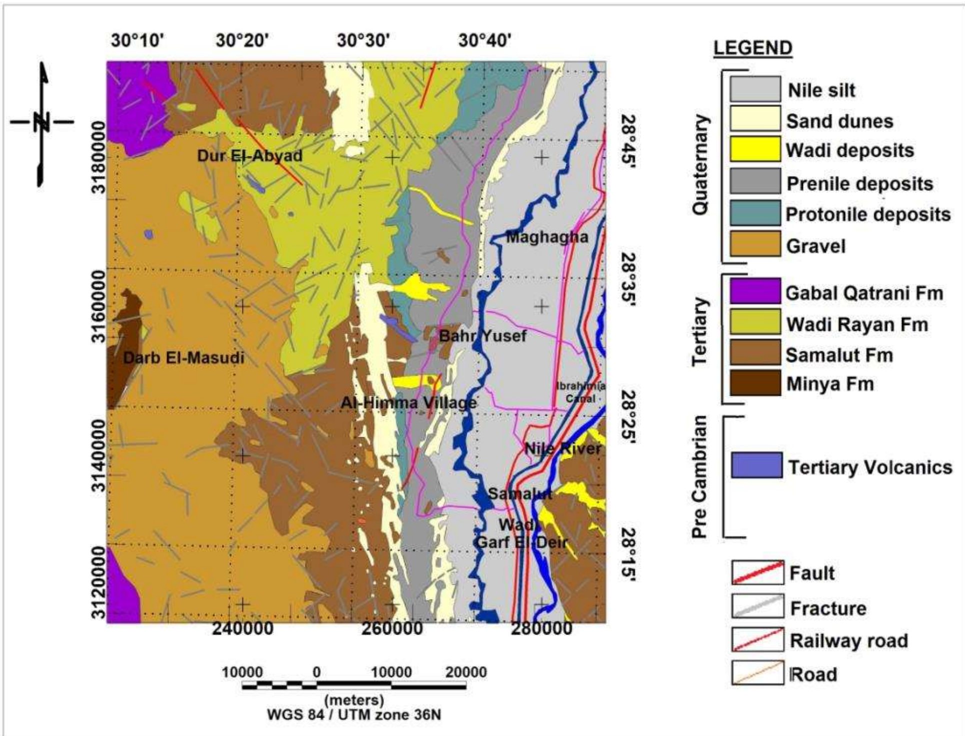

Figure 2: Geologic map of the study area (After Conoco, 1987).

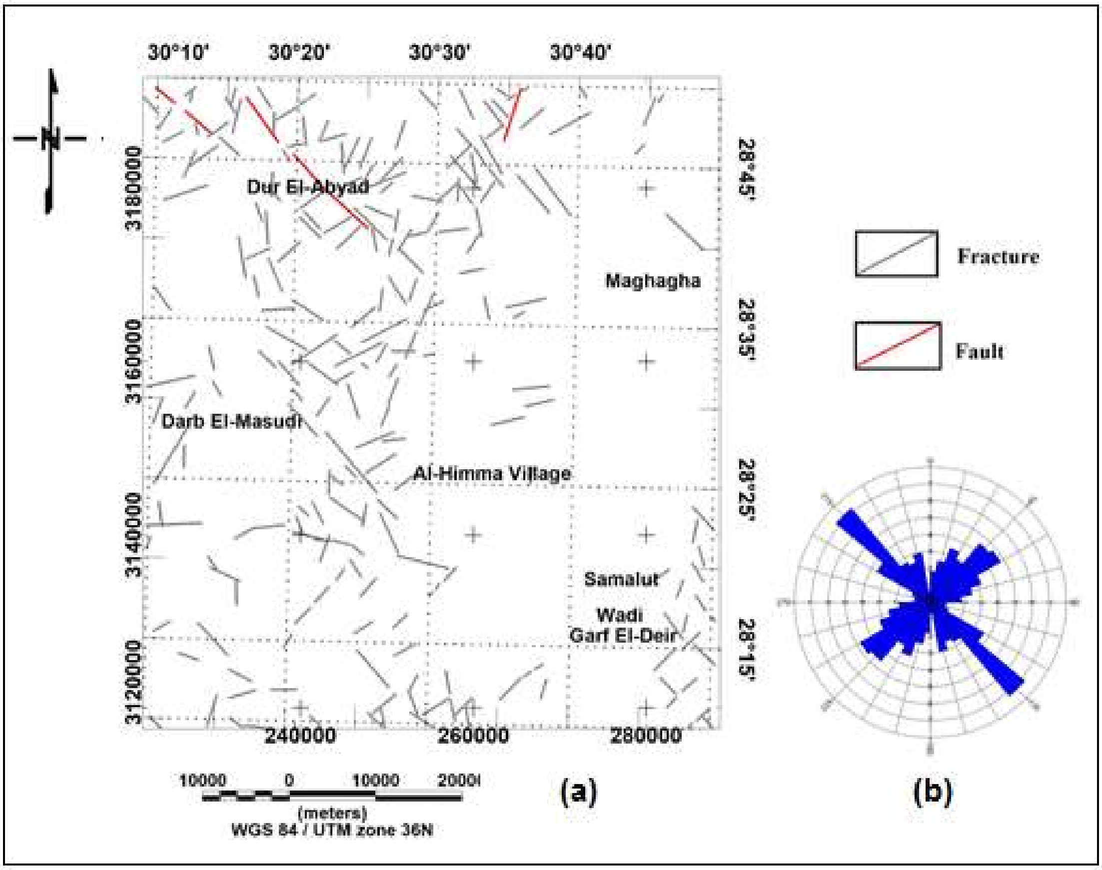

Figure 3: a) Geologic fault trends and fractures derived from the geologic map of the study area in figure (1) and b) Rose diagram of the geologic lineaments of the study area (Conoco, 1987).

METHODOLOGY

1- Remote sensing data

The remote sensing data are available for downloading from http://earthexplorer.usgs.gov website. In the current study, the Digital Elevation Model (DEM) representing the surface of the area under investigation. The DEM was processed for geomorphological analysis and to determine the hydrological basins as well as to delineate surface structure which exists in the study area.

2- Magnetic data

Magnetic data of the area under investigation were derived from the Earth Magnetic Anomaly Grid (2-arc-minute resolution) (Meyer et al, 2016). The Oasis Montaj ™ software package (version 6.4.2) was used in the processing and interpretation of the data.

3- Vertical electrical sounding (VES) and drilled well

Three vertical electrical sounding (VES) were acquired in the study area using Schlumberger array, and a well was drilled by Green Valley Company for monitoring wells (Fig. 4 and Table 1). The half current electrode spacing (AB/2) of VES's starts from one meter to 400 meters. Field photo and resistivity field instruments (GR resistivity instrument, wires, hammers and steel electrodes) are shown in Figure 5.

Table 5: Locations of the VES's and drilled well within the study area.

VES's and drilled well	Lat	Long
VES no (1)	28° 28' 10.45"N	30° 36' 34.47" E
VES no (2)	28° 28' 10.7" N	30° 36' 39.45" E
VES no (3)	28° 28' 11" N	30° 36' 43.66" E
Drilled well	28° 27' 13.90" N	30° 35' 16.81" E

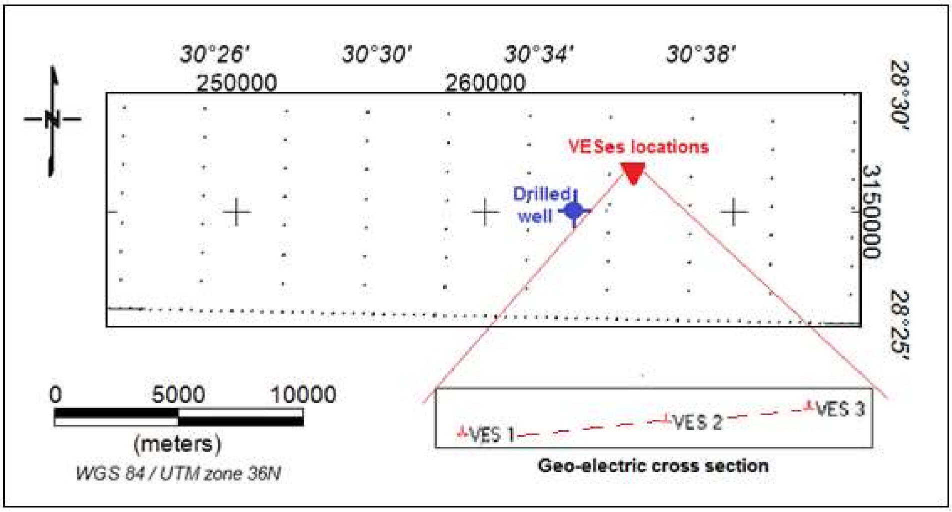

Figure 4: Location map of the drilled well, VES's and geoelectric cross section in the study area.

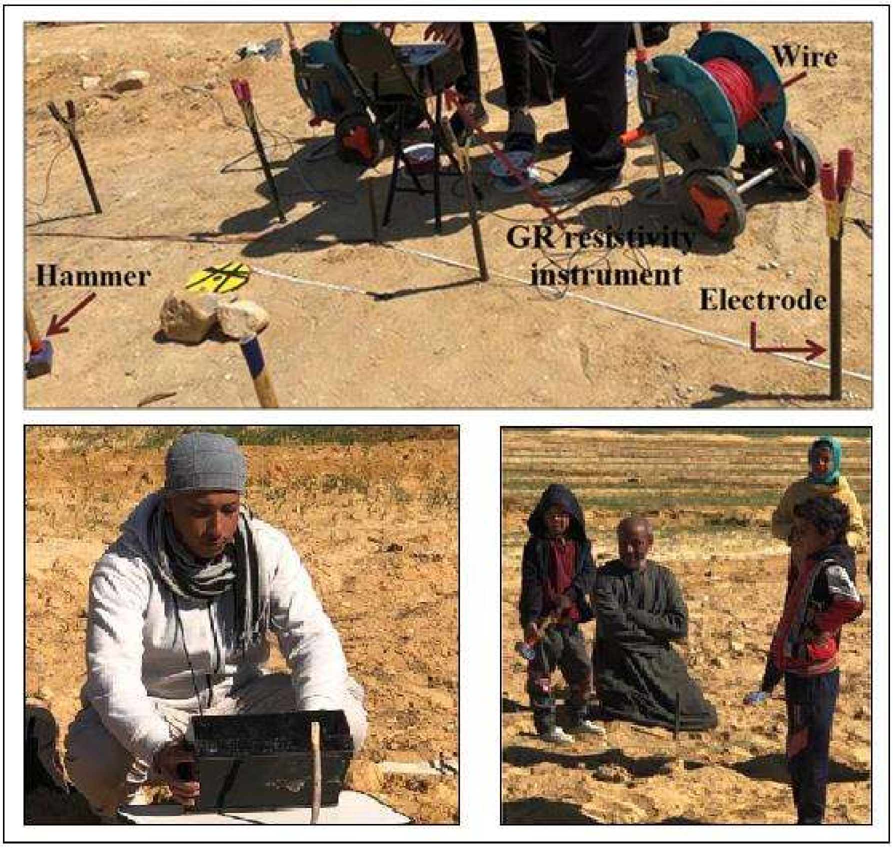

Figure 5: Field photo and resistivity field instruments.

RESULTS AND INTERPRETATION

1- Surface analysis using DEM data

1.1- Elevation

The topographic elevation map (Fig. 6) shows that the high elevations (more than 170 m) occur at the NW part of the area, while the low elevations (less than 50 m) are located at the NE, E, and SE parts of the study area.

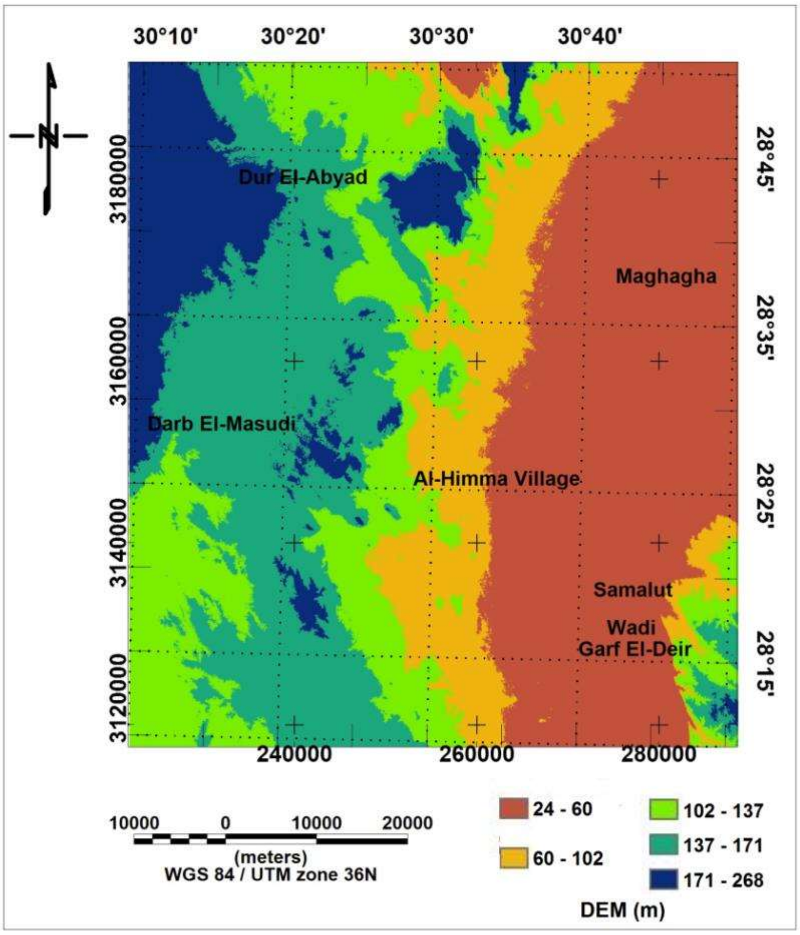

Figure 6: Digital elevation model (DEM) of the study area (http://earthexplorer.usgs.gov).

1.2- Stream orders

Pareta and pareta (2012) stated that the stream orders technique is used to detect the drainage patterns. The investigated area contains ten basins and seven streams. Each one from these streams was discriminated by different color as shown in figure 7.

1.3- Lineaments extraction

The first step is represented by the shaded relief images generated from the DEM with different sun angles (from 0° to 315°). Combined maps represent the second step by; combining the first four shaded images (0°, 45°, 90° and135°) to produce one image and combining the other image (180°, 225°, 270° and 315°) to produce one image (Fig. 8). The extracted lineaments from the combined images were found to strike in the NW-SE, N-S and NE-SW directions (Figs. 9 and 10).

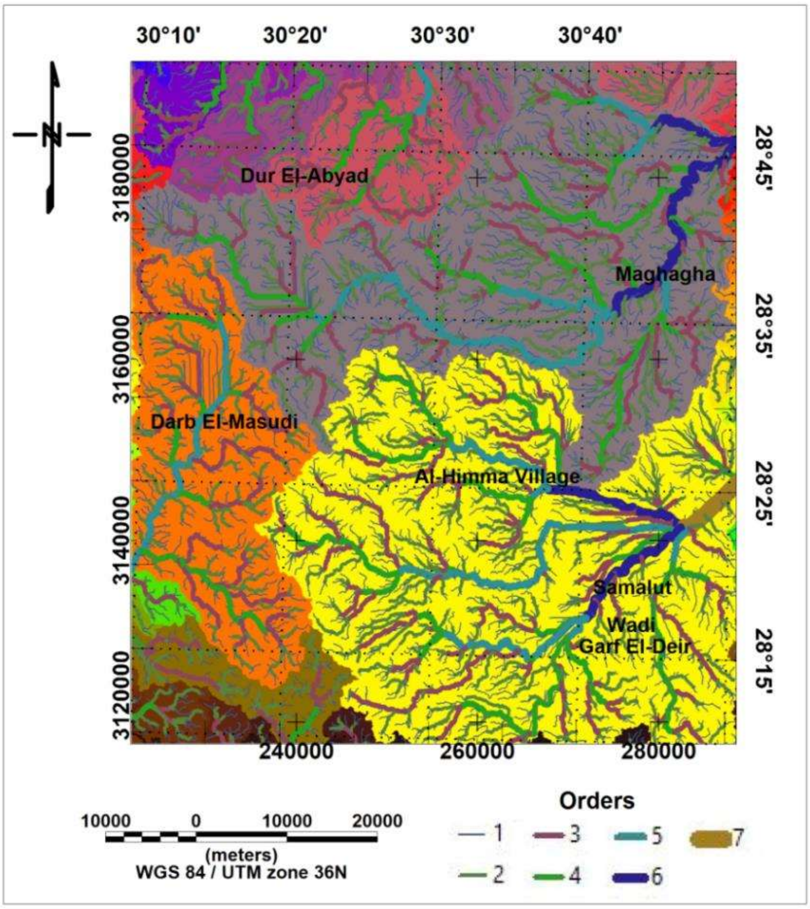

Figure 7: Stream order within the basins of the study area.

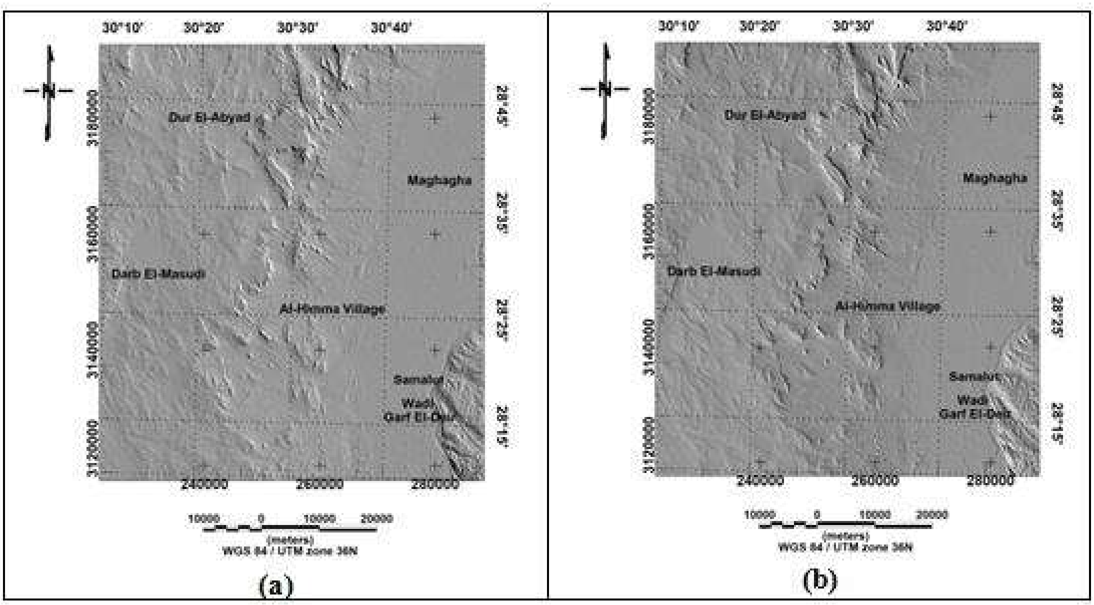

Figure 8: a) Shaded relief image created by combining four shaded relief images with sun angles of 0, 45, 90, and 135. b) Shaded relief image created by combining four shaded relief images with sun angles of 180, 225, 270, and 315 of the studyarea.

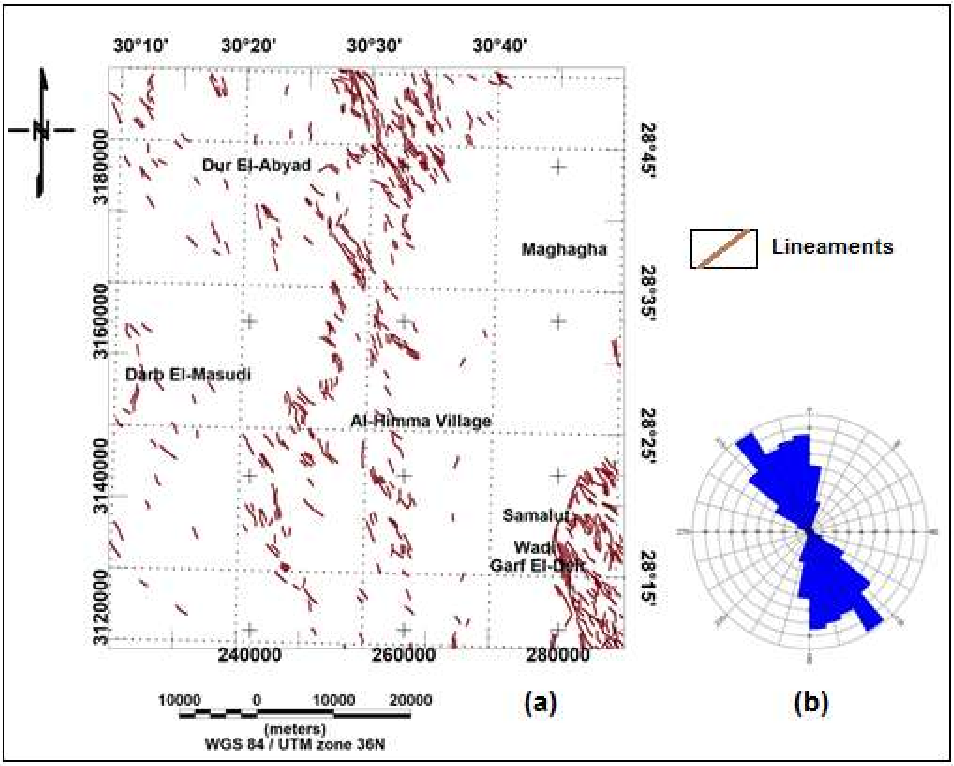

Figure 9: a) Automatic lineament map of combining four shaded relief images with sun angles of 0, 45, 90, and 135 and b) Rose diagram of the automatic lineament map of the study area.

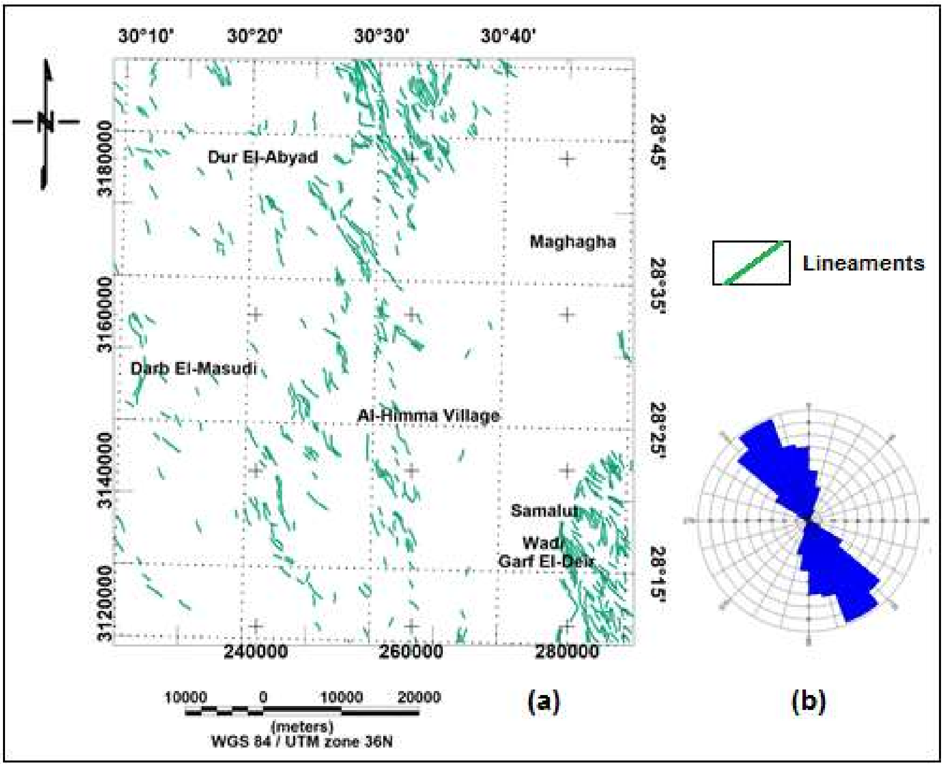

Figure 10: a) Automatic lineament map of combining four shaded relief images with sun angles of 180, 225, 270, and 315 and b) Rose diagram of the automatic lineament map of the study area.

2- Interpretation of magnetic data

2.1- Total magnetic intensity (TMI) map

The total magnetic intensity (TMI) map (Fig. 11) reveals that, the central and SE parts of the study area are occupied by low and moderate magnetic values (less than 5 nT). The northern and SW parts of the area are occupied with high magnetic values which range between 5 nT to > 37 nT.

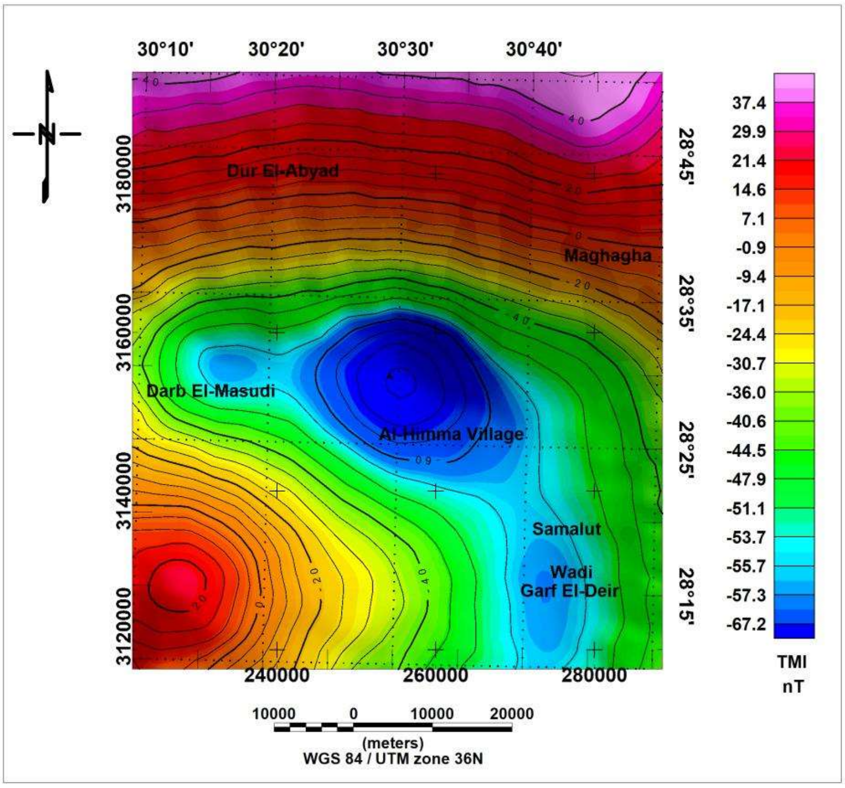

Figure 11: Total magnetic intensity (TMI) map of the study area.

2.2- Reduced to the north magnetic pole (RTP)

Inspection of RTP map (Fig. 12) shows that, the NE, NW, W and SW parts of the area represent the high magnetic values that ranging from 5 nT and reaching to more than 43.2 nT. The intermediate magnetic values (from -30 to 5 nT) are located at the central and parts of the NW side of the area. The northern, central and southern parts of the area are occupied with low magnetic values (less than -30 nT).

2.3- Radially averaged power spectrum

This technique calculates the average depths (h) of the residual and regional sources using the following formula:

$$h = -slope/4\pi \qquad \text{Equation (1)}$$

Figure (13) shows two main average levels (interfaces) at depths 2.5 Km (near surface) and at 7 Km (deep seated) below the measuring level.

2.4-Regional and residual magnetic maps

The investigation of the low-pass filtered (regional) map (Fig. 14) reveals that; the northern, central and southern parts with less than zero values represent the low magnetic zones, while the high magnetic anomalies present at the NE, NW, W and SW parts of the area. The regional magnetic map shows the presence of many basins with a thick sedimentary cover at the northern, central and southern parts of the investigation area. VES's and drilled well are located inside the central sedimentary basin. The high-pass filtered (residual) map (Fig 15) shows some anomalies originated from shallow sources such as; southern and central parts and disappear at the regional map.

2.5- First vertical derivative (FVD)

This technique is used to detect the edges and boundaries of geologic bodies (Henderson and Zietz, 1949). Figure (16) (FVD map) shows that; the main trends of geologic bodies take NW-SE and NE-SW directions.

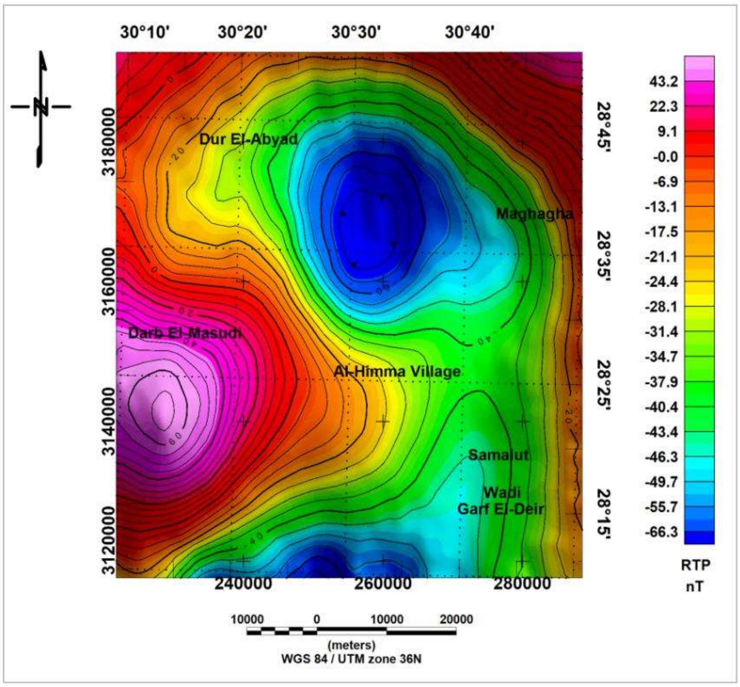

Figure 12: Reduced to the northern magnetic pole (RTP) Map the study area.

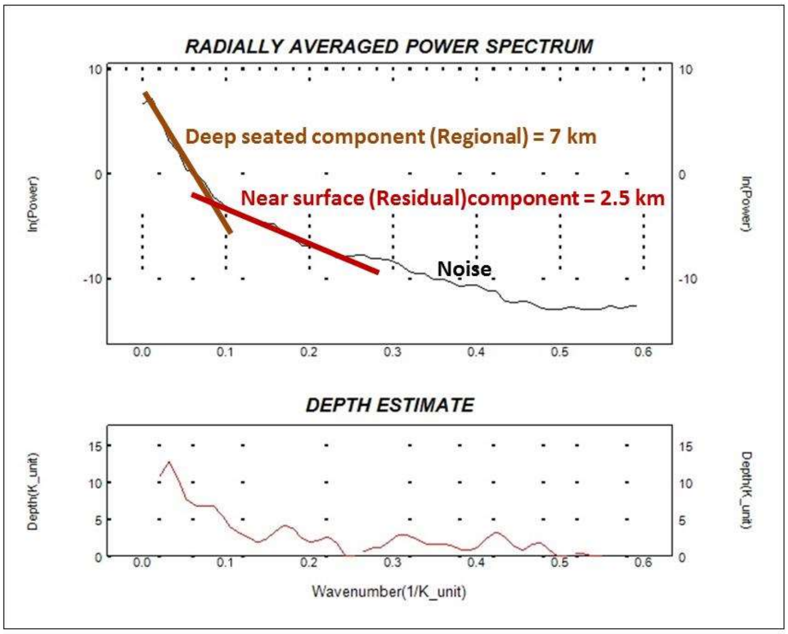

Figure 13: Radially averaged power spectrum and depth estimate of magnetic data of the study area.

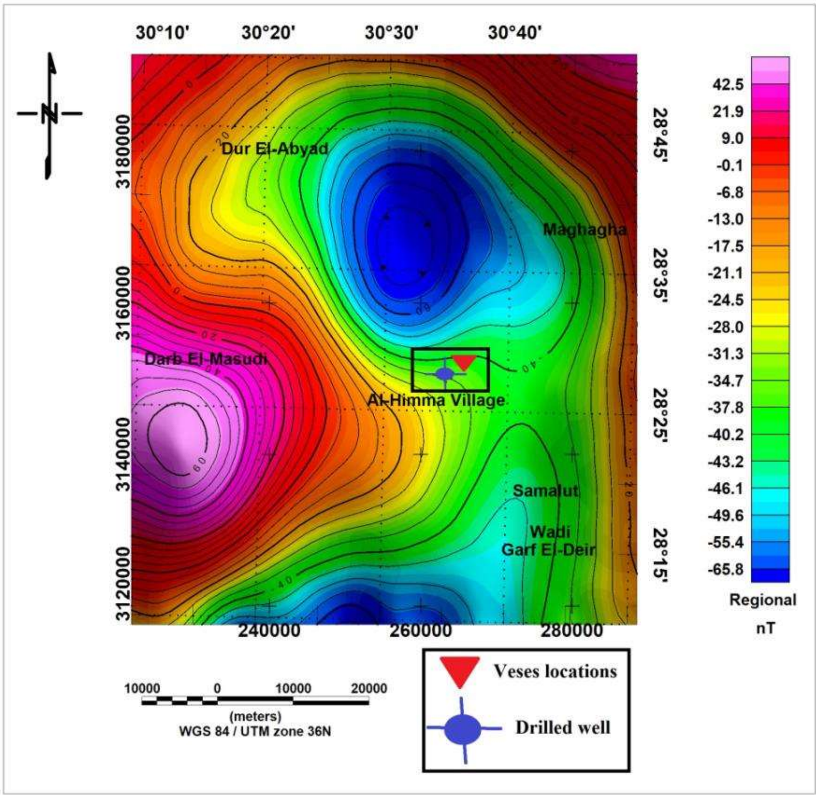

Figure 14: Locations of drilled well and VES's inside the study area plotted on regional magnetic map.

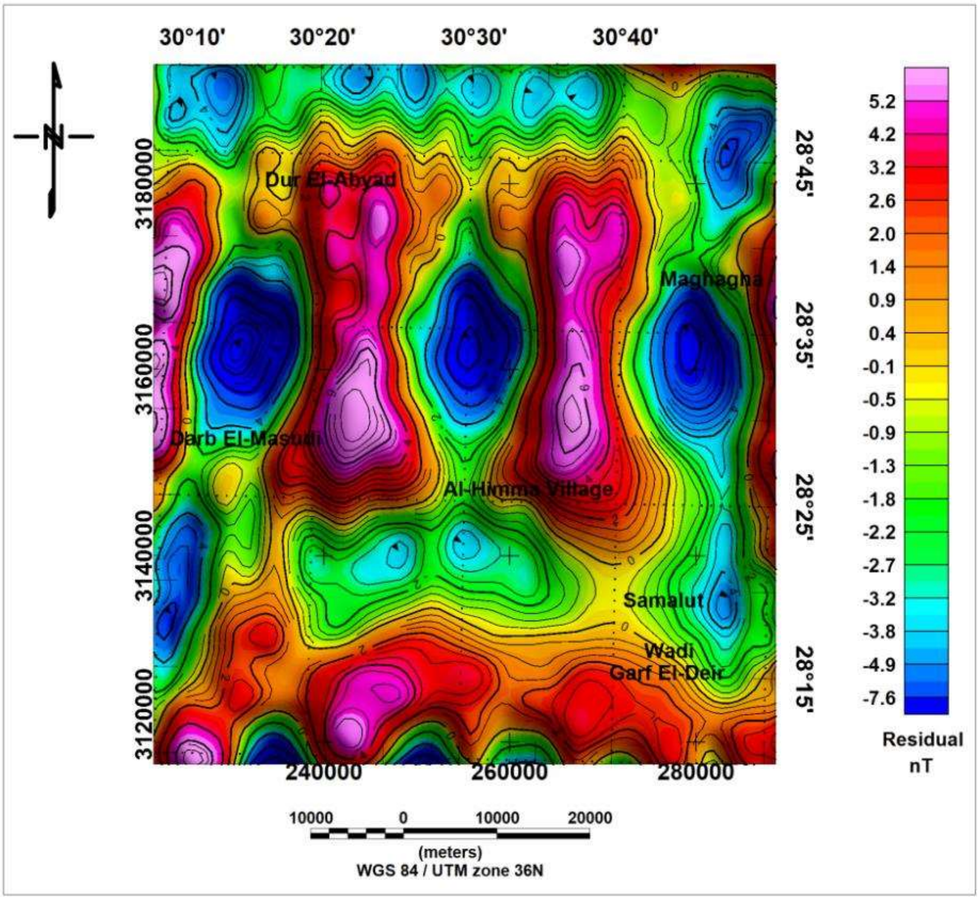

Figure 15: Residual magnetic anomaly map of the study area.

2.6- Euler deconvolution

Depth estimation of the area under investigation was conducted by Euler deconvolution. The Euler solutions using a structural index (SI) =0 for detecting contacts are represented in figure (17). This figure reveals that the subsurface contacts depths range between < 1686 m and > 5393 m.

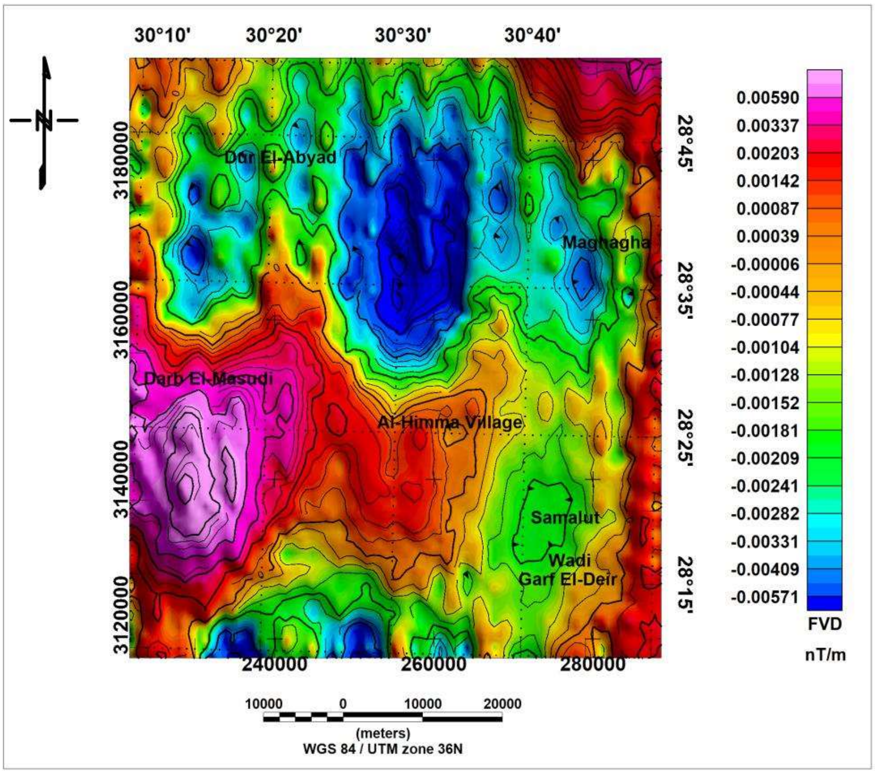

Figure 16: First vertical derivative map of the study area.

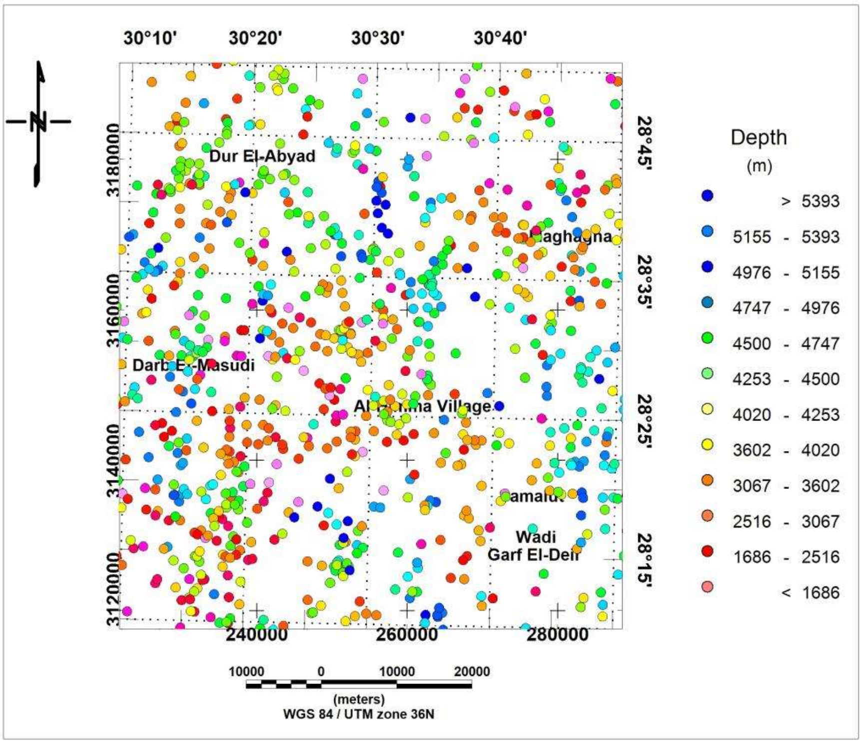

Figure 17: Euler deconvolution technique of the study area.

2.7- Structural Interpretation

The interpreted magnetic structures maps (Figs. 18 & 19) of the area under investigation were created using geologic background, as well as the results obtained from the geophysical tectonic trend analysis. The structural lineaments of these maps strike in the N-S, E-W, NE-SW and NW-SE directions.

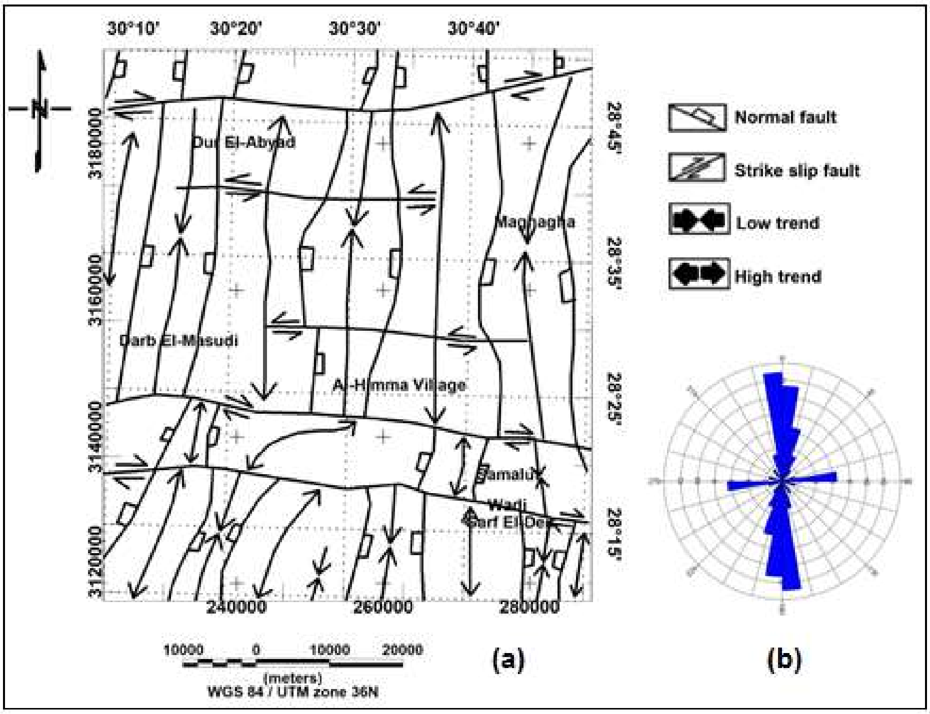

Figure 18: (a) Shallow structural elements magnetic map and (b) rose diagram of shallow structural elements of the study area.

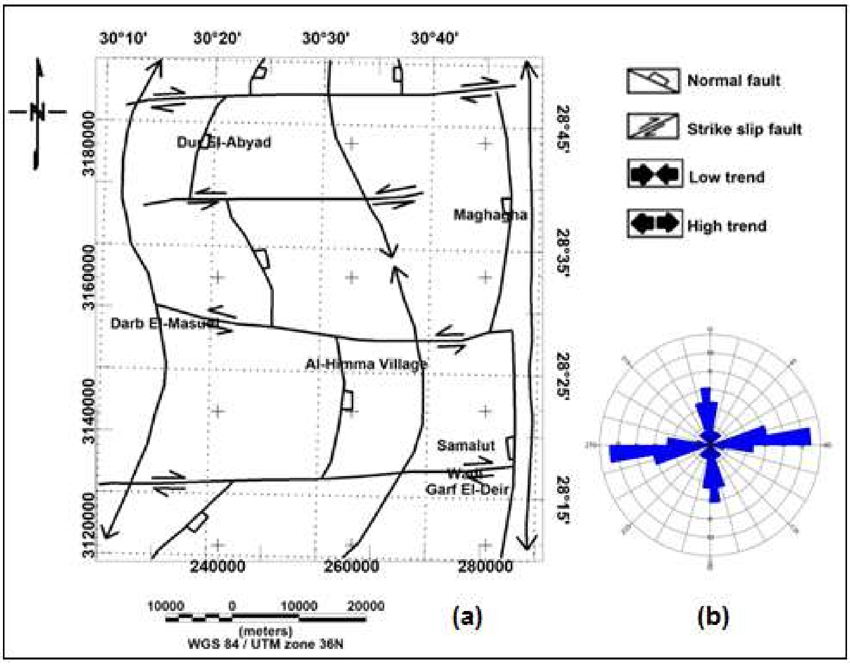

Figure 19: (a) Deep-seated structural elements magnetic map and (b) rose diagram of deep-seated structural elements of the study area.

3- Analysis and interpretation of VES's and drilled well data

3.1- Data analysis and interpretation

Ato program (Zohdy and Bisdorf, 1989) and Resist program (Velpen, 1988) geoelectric resistivity softwares were used to analyze and interpret the geoelectric data (Fig. 20) and the VES's results are summarized in Table (2). The VES's results reflected that; the unconsolidated wadi sediments represent the first layer with average thickness of 2.2 m and resistivity values reaching to more than 200 Ω.m. The second geoelectric layer is characterized by clay stone, which has average thickness of 7.1 m and resistivity of 6.2 Ω.m. Intercalation of clays and sands represented the third layer with resistivity values ranging from 72.6 to 166.6 Ω.m and thickness of 7.6 m. The fourth geoelectric layer represents the good aquifer, which is composed of fractured limestone with average resistivity of 885.1 Ω.m. Geoelectric cross section (Fig. 21), provides information about the subsurface setting. The subsurface succession of the drilled well (Fig. 23) includes from the top to bottom wadi deposit, claystone, and limestone with clay intercalation. The water level starts at 12.5 meters with a salinity of 1645mg/l, suitable for agriculture purposes and fish farms.

3.2- Results integration

Figure (22) shows the outcrop of wadi deposits and the upper part of clay bed, which matches with the geoelectric results. Figure (23) summarizes the subsurface succession using a brief correlation between VES 1 and the drilled well in the investigated area.

Table 2: Resistivity parameters of geoelectric layers.

VES No.	Parameters	Geoelectric Layers			
		1	2	3	4
VES 1	Resistivity (Ohm.m)	46.6	9.5	72.6	415
	Thickness (m)	1.1	13.4	7.8	17.3
	depth (m)	1.1	14.5	22.3	39.6
VES 2	Resistivity (Ohm.m)	218.9	3.3	109.2	848.5
	Thickness (m)	0.9	2.7	7.5	49.3
	depth (m)	0.9	3.6	11.1	60.4
VES 3	Resistivity (Ohm.m)	23.5	5.9	166.6	1391.8
	Thickness (m)	4.6	5.2	7.4	41.7
	depth (m)	4.6	9.8	17.2	58.9

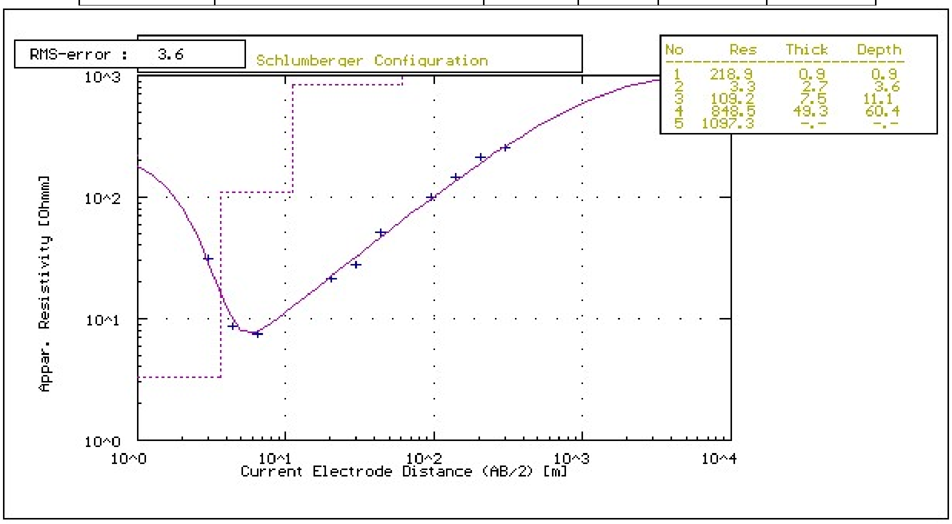

Figure 20: Geoelectric layer modeling of VES no.2 as an example.

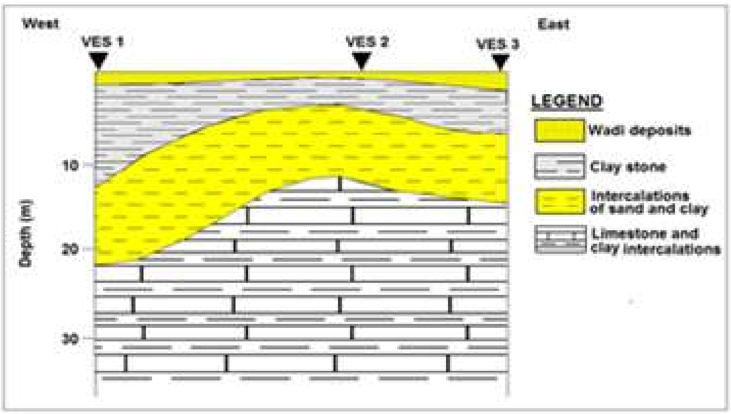

Figure 21: 2D geoelectric cross section passed through VES's 1, 2 and 3

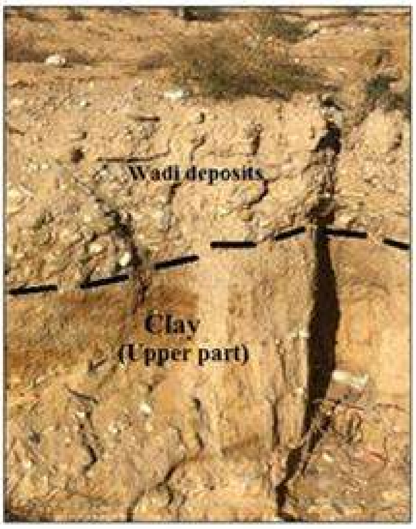

Figure 22: Outcrop of wadi deposits and the upper part of the clay bed.

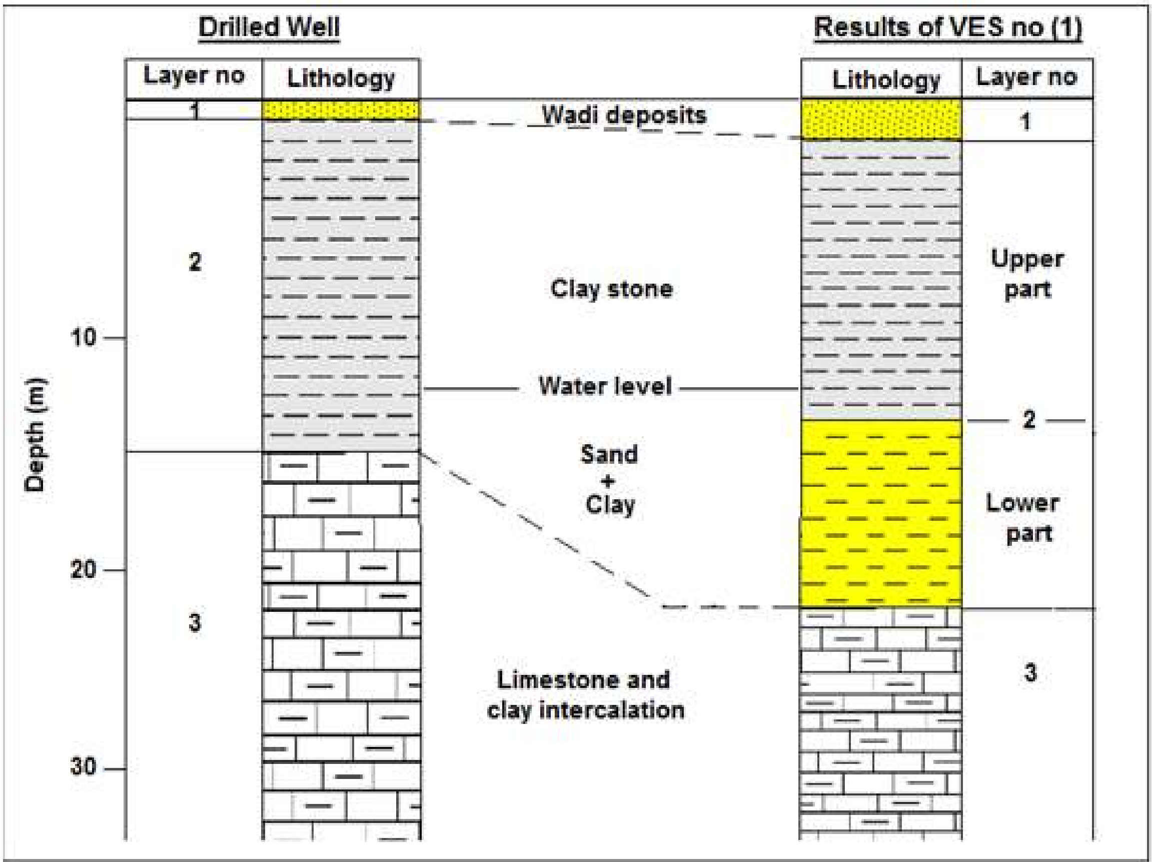

Note that; 1) The distance between drilled well and VES no (1) reaches to 2.7 km.
2) The drilled well is located south of VES no (1).
3) The depth of the limestone layer decreases towards the south direction.
4) Sand and clay layer disappears towards the south direction.

Figure 23: Correlation between geoelectric results of VES no (1) and drilled well data inside the study area.

CONCLUSIONS

The area under investigation is one of the key areas that are targeted for future national development and investment plans. Surface lineaments could be detected by DEM shading and field geology, while subsurface lineaments could be detected by magnetic data. Surface and subsurface lineament are found striking N-S, E-W, NW-SE and NE-SW directions. Subsurface lithology of the study area is represented by unconsolidated sediments, claystone, intercalation of sand and clay and fractured limestone that represents the subsurface aquifer layer.

REFERENCES

Abdullah A. Z. and Ahmed A. S., 2021, Effects of Topographic factor and Geomorphologic Features on Soil Characteristics of the Western Area of Bahr Yousef, El-Minya, Egypt. Ass. Univ. Bull. Environ. Res. Vol. 24 No.

Abouelmaged R. G., Barseem M. S. M., Metwally S. E. M., Farag, M. S. M. and Mousa S. E. A., 2020, Groundwater Exploration in Fractured Rocks Using Transient Electromagnetic Technique (TEM), West El-Minia, Egypt. Egyptian Geophysical Society. EGS Journal, Vol. 18, No. 1, 145-154

Abdelaal A. M., Sameah S. and Ahmed A., 2017, Characterization of Calcium Carbonate Rocks, East El Minya Deposits for Possibility Uses as Industrial Raw Materials. Journal of Petroleum and Mining Engineering.

Asmoay A., Mousa I. and Mohamed A., 2024, Appraisal of Heavy Metal Content in the Groundwater at W-W El Minya District of Egypt. Egypt. J. Chem. Vol. 67 No. 3 pp. 169 – 180. http://ejchem.journals.ekb.eg/.

Conco, 1987, Geological map of Egypt, Scale 1: 500 000, NH 36 SW, Beni Suef Sheet.

Darwish K., 2023, GIS-Based Multi-Criteria Decision Analysis for Flash Flood Hazard and Risk Assessment: A Case Study of the Eastern of Minya Area, Egypt. Environ. Sci. Proc. https://doi.org/10.3390/xxxxx.

Gedamy Y., Abdulhady Y. and Zaghlool E., 2019, Hydrochemistry of the Eocene Aquifer at the Desert Fringes of West El-Minya Governorate, Egypt. Curr. Sci. Int., 8(4): 734-763, 2019. EISSN: 2706-7920 ISSN: 2077-4435. DOI: 10.36632/csi/2019.8.4.15.

Henderson, R. G. and Zietz, I., 1949, The Computation of Second Vertical Derivatives of Geomagnetic Fields. Geophysics, Vol. 14.

Meyer B., Richard Saltus., Arnaud Chulliat., 2016, EMAG2: Earth Magnetic Anomaly Grid (2-arc-minute resolution) Version 3. National Centers for Environmental Information, NOAA.

Moftah H., Hassan H., Moustafa A., Mohamed A., Ali M. A. and Abdellah W. R., 2022., Geological studies and engineering applications of some Middle Eocene carbonate rocks in East The Minia Area, Egypt. Arabian Journal of Geosciences. https://doi.org/10.1007/s12517-022-10915-8.

Pareta K. and Pareta U., 2012, Quantitative Morphometric Analysis of a Watershed: Based on Digital Terrain Model and GIS. LAP Lambert Academic Publishing, Germany, 1-93.

Shabana, A.R., 2010, Hydrogeological studies on the area west Deir Mouas-Mallawi, El-Minya governorate, Egypt. Egyptian journal of geology, 54: 61-78.

Velpen, B. P. A., 1988, Resist program, V. 1.0. M.Sc Research project, ITC, Holland.

Zohdy, A. A. R., and Bisdorf, R. J., 1989, Programs for the automatic processing and interpretation of Schlumberger sounding curves in Quick Basic; U.S. Geological Survey Open File Report 89-137-2, 64 p.

Websites: http://earthexplorer.usgs.gov.

8. ACKNOWLEDGEMENTS

Great thanks are expressed to Prof. Dr. Ahmed Abu El-Ata Professor of Applied Geophysics, Geophysics Department, Faculty of Science, Ain Shams University and Dr. Ahmed Al Dabour, Green Valley Company for monitoring wells; for cooperation and great help to complete this work.